Article

Idarubicin−Gold Complex: From Crystal Growth to Gold Nanoparticles

Carole Barbey, Nadia Bouchemal, Pascal Retailleau, Nathalie Dupont, and Jolanda Spadavecchia*

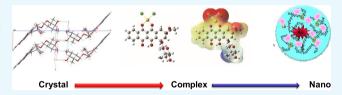Cite This: *ACS Omega* 2021, 6, 1235−1245

Read Online

ACCESS | Metrics & More | Article Recommendations | SI Supporting Information

ABSTRACT: Idarubicin (IDA) is the analog of daunorubicin (DNR). The absence of the methoxy group at position 4 of IDA remarkably improved lipophilicity, which is responsible for extra cellular uptake, higher DNA-binding ability, and considerable cytotoxicity in correlation with doxorubicin (DOX) and DNR. In this paper, we conceived two principal objectives: we realized the crystal structure of IDA by X-ray diffraction measurements on single crystals at room temperature (monoclinic, space group $P2_1$, a = 5.1302(2) Å, b = 9.9122(5) Å, c = 24.8868(11) Å; β = 91.425(4)°; V = 1265.14(10) Å^3) with refinements of the structure converged to the final R = 3.87%. The second objective has been to develop gold nanoparticles encapsulated with idarubicin through an original methodology in which gold salt ($HAuCl_4$) is chelated with IDA and diacid polymer (PEG) to form hybrid nanoparticles called IDA IN PEG-AuNPs in which drug solubility was enhanced. The computational studies were in agreement with the experimental observations. These hybrid nanoparticles and their precursors were analyzed by Raman, UV−Vis, ^{1}H NMR, and transmission electron microscopy (TEM). The main results are completed by a theoretical approach to understand the whole process.

INTRODUCTION

Anthracyclines (Scheme S1 in the Supporting Information) are an important class of chemotherapeutic agents that have been synthesized over the years to improve the clinical properties.[1] Their clinical benefit, however, is sometimes hampered by the development of cardiotoxicity, a process that still remains under investigation.[2]

Anthracycline analogs vary by the substitution patterns on the chemical units, which confer a different anticancer activity and cardiotoxicity.[1] For instance, doxorubicin (DOX) and its semisynthetic C-4′ sugar epimer epirubicin (EPR) exhibit a modest variation in antitumor efficacy, but EPR causes less cardiac harm.[3,4]

The first aim of this work was to determine the crystal structure of IDA itself, which has never been reported until now. Indeed, a Cambridge Structural Database (CSD version 5.40)[5] search for the IDA skeleton structure offers no results. However, little crystal structures of IDA linked to DNA, enzymes, and proteins have been related in the literature and an RCSB Protein Data Bank[6] search gave only five published crystal structures of these molecules with IDA as a ligand (DM5 ligand code in PDB) (PDB ID: 3ARQ, 4LB2, 198D, 1D67, and 1D38). A Cambridge Structural Database (CSD version 5.40)[6] search for idarubicin gave no hits. So, in the absence of a high-resolution crystal structure, we have determined this to be (7S-cis)-9-acetyl-7-[(3-amino-2,3,6-trideoxy-α-L-lyxo-hexopyranosyl)oxy]-7,8,9,10-tetrahydro 6,9,11-trihydroxynaphthacene-5,12-dione chloride.

Nowadays, more studies concern the development of drug's hybrid gold nanovectors. Previously, Moustaoui et al. have conceived a novel hybrid nanoparticle based on a gold−doxorubicin complex named DOX IN-PEG-AuNPs.[7] In this nanoparticle, doxorubicin (DOX) and PEG diacid react with Au (III) ions from gold salt ($HAuCl_4$) by chelation reaction. This chemical methodology has been applied to any drugs with a capacity of complexation as described previously.[8,9]

Theoretical DFT-based studies are considered from the molecular anthracycline isolated system to the first step of nanoparticle growth on the basis of experimental results to offer a better understanding of the phenomenon. The second aim of this research is to realize a novel nanodrug using idarubicin (IDA) chelated to gold ions to obtain nanoparticles (IDA IN-PEG-AuNPs). This hybrid nanovector will be extensively used as chemotherapeutic agents against cancer cells due to their high stability. We provide that this study will take a strategic place in the field of structural nanomedicine. To the best of our knowledge, these results have never been realized before in published papers.

RESULTS AND DISCUSSION

Structure of Idarubicin Hydrochloride Salt. Idarubicin crystallizes in the noncentrosymmetric $P2_1$ space group (no.

4). A complete data set was collected with 12,425 reflections integrated in the θ range of 3.28° to 29.09°, of which 5296 were unique, leaving an overall R merge of 0.0460 and an overall completeness of 99.50%. For solution and refinement, 3183 reflections were considered to be unique after merging for Fourier. For other details concerning the crystal data, data collection is given in Table 1. The final agreement factors were

Table 1. Crystallographic Data and Refinement Data

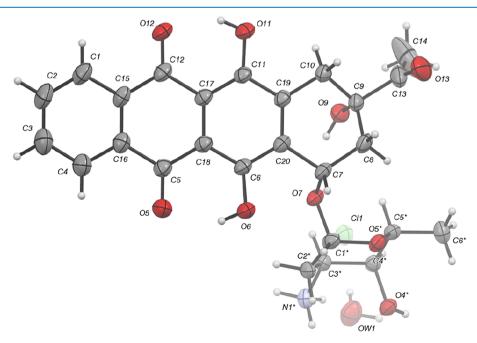|	
chemical formula	$C_{26}H_{28}NO_9{}^+$, Cl^-, H_2O
formula mass	551.96 g·mol^{-1}
crystal system	monoclinic
a (Å)	5.1302(2)
b (Å)	9.9122(5)
c (Å)	24.8868(11)
β (°)	91.425(4)
unit cell volume (Å^3)	1265.14(10)
crystal size, color	0.1 × 0.03 × 0.01 mm, orange
temperature (K)	293 (2)
space group	$P2(1)$
Z	2
radiation	Mo Kα (λ = 0.71073 Å)
θ range for data collection	3.28° to 29.086°
reflections collected/unique/with [$I > 2\sigma(I)$]	12,425/5296/4738
data/restraints/parameters	5296/13/362
goodness of fit on F_2	1.041
final R indices [$I > 2\sigma(I)$]	R_1 = 0.0387, wR_2 = 0.0937
R indices (all data)	R_1 = 0.0440, wR_2 = 0.0958
$(\Delta\rho)$max	0.286 e·Å^{-3}
$(\Delta\rho)$min	−0.222 e·Å^{-3}
CCDC deposition number	2027730

R_1 = 0.0387 for 4738 reflections with $I > 2\sigma(I)$, R_1 = 0.0440 and wR_2 = 0.0958 for all 5297 data, and G.O.F. (goodness of fit of a statistical model) = 1.041. The residual electron density in the final difference Fourier was of no chemical significance.

The asymmetric unit is composed of one protonated IDAH$^+$ cation, one Cl$^-$ anion, and one water molecule. An Oak Ridge Thermal Ellipsoid Plot (ORTEP) program view with a numbering scheme of the asymmetric entities is given in Figure 1. The IDAH$^+$ ion consists of an aglycone tetracycle attached to a sugar moiety in a chair conformation. The two intramolecular H-bonds observed between a quinone oxygen and hydroquinone hydroxyl are the best conformational characteristic, obtaining the stability of the aromatic backbone conformation: one between C5−O and C6−OH and the other between C12−O and C11−OH (Table 2). The C8 carbon is

Table 2. Intramolecular Hydrogen Bond Parameters (Distances in Å and Angles in °)^a

D−H	d (D−H)	d (H···A)	<DHA	d (D···A)	A
O6−H6	0.820	1.860	145.5	2.578 (3)	O5
O11−H11	0.820	1.829	145.5	2.545 (3)	O12
O9−H9	0.820	2.186	146.4	2.906 (3)	O7
N1*−H03C	0.900	2.442	153.0	3.270 (2)	Cl1 (a)
OW1−H1W	0.890	2.294	175.01	3.185 (3)	Cl1 (b)

^{a}Symmetry transformations used to generate equivalent atoms: (a) −x + 1, y − 1/2, −z + 1; (b) x − 1, y, z.

hardly coplanar on the anthracycline plane (C19−C20−C7−C8 torsion angle is 7.58°). The functional group at C9 is above the anthracycline plane with a C20−C19−C10−C9 torsion angle of 22.96°. This conformation at C9 is stabilized by H-bond formed between C9−OH and O4 (Table 2). The C7-connected daunosamine is the conformational entity shown in all anthracyclines.[26,27] The N3*−O7 distance of 4.423 Å is in accordance with the density functional theory-calculated diversity (2.71 to 8.44 Å).[28] The ammonium group forms a hydrogen bond with the chloride counterion with a N···Cl distance of 3.270 Å. The distances and angle are consistent with those reported (Table 2).[29]

Figure 1. Molecular view of the asymmetric unit content of idarubicin with atom labels. Displacement ellipsoids are drawn at the 50% probability level, and H atoms are shown as small spheres of arbitrary radii.
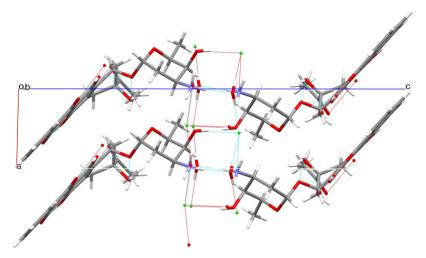
Figure 2. Molecular packing of idarubicin projected over the crystallographic *b* axis. Aromatic rings stack in a parallel plane and form slices to the *a* axis with connectivity, ensuring an extensive bond network.
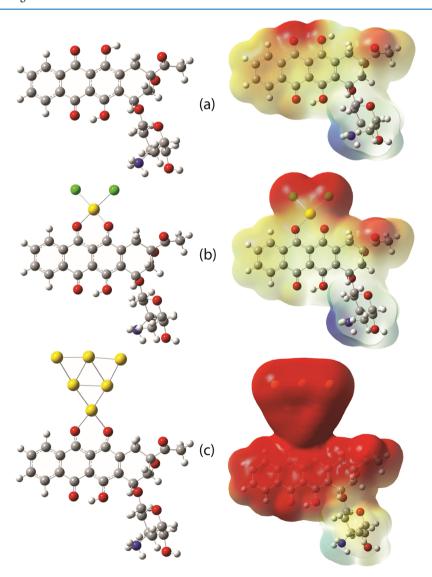

Figure 3. Structures considered in the theoretical study and the corresponding electrostatic potential maps on total density (MESP). (a) sI: idarubicin alone; (b) sII: dichloro Au (III)−idarubicin complex; (c) sIII: system associating a small Au_6 cluster and an idarubicin molecule. On MESP, the potential is represented with a color scale from a red color corresponding to the zero value to a blue color corresponding to the most positive value.

Supramolecular Features. Two symmetric entities of IDA form a dimer via an extensive network of intermolecular water or chloro-mediated hydrogen bonds. The packing of the crystal is depicted in Figure 2.

The crystal structure consists of layers, parallel to the [100] direction, of hydrophobic regions that enclose the tetracyclic moiety of idarubicin and polar regions where the ammonium group and chloride counteranion are involved in an extensive bond network, mediated by a water molecule. The tetracyclic plane platform plays a key role in the cohesion of the crystal structure by realizing slices alongside the *a* axis via favorable intermolecular $\pi-\pi$ stackings (centroid-to-centroid distances: 3.619 and 4.323 Å).[30] Strong intermolecular hydrogen bonds cross-link these slices perpendicularly, producing a two-dimensional network parallel to (100). Distances indicating centroid measurements and also figures have been done using CCDC CSD Mercury 2 software.[31]

Theoretical Study of Idarubicin Isolated System and Idarubicin−Gold Complex. As described for doxorubicin in our previous study,[7] DFT (density functional theory) and TD-DFT (time-dependent density functional theory) calculations can be used to analyze the electronic, spectroscopic, and geometric properties deduced from the optimized structures in vacuum and in water for idarubicin isolated system sI, dichloro Au (III) complex sII, and a system associating a small Au$_6$ cluster and an idarubicin molecule sIII representing the first step of nanoparticle growth (Figure 3).

After full geometry optimizations in vacuum and water, comparison of the calculated and experimental geometrical parameters reveals only minor differences; thus, the optimized structure has been used for further theoretical analysis and descriptor computation. To search for the best anthracycline in anticancer activity and cardiac tolerability,[32,33] there is a need of knowledge completion on the current analogs and their complexes. Molecular quantum modeling can give access to some adequate quantum descriptors such as frontier orbital HOMO and LUMO energies, energy gap, dipolar moment, global hardness, and molecular polarizability α.[34−36] The final goal of such structure−activity relationship (SAR) studies is frequently the correlation of the biological affinity of a series of analog compounds with several descriptors to support the understanding of the phenomenon and eventually the design of new active systems.

The chemical descriptors for idarubicin and doxorubicin are listed in Table 3. As the two analogs have very similar structures, most of the descriptor values are very close with less than 0.5% difference. As polarizability measures the ability of electron density to be influenced by an external stimulus, the harder a molecule is, the lower is its average polarizability. Computed total α polarizability is approximately 6% higher for doxorubicin. The dipole moment in Debye results from a non-uniform charge distribution on several atoms in a given molecule. The computed dipolar moment is approximately 2% higher for idarubicin.

The frontier molecular orbitals HOMO and LUMO guide the interaction of a molecule with other species. Higher values of HOMO energy are related to the greater ease of donating electrons to the unoccupied orbital of the receptor. The smaller the value of LUMO energy is, the smaller the resistance to accept electrons will be. According to Koopman's theory, ionization energy *I* and electron affinity *A* can be directly expressed through respective absolute values of HOMO and LUMO energies.[37] The gap ΔE in energy between the HOMO

Table 3. Chemical Descriptors of Idarubicin and Doxorubicin Molecules[a]

chemical descriptor	idarubicin	doxorubicin
HOMO energy (in H)	−0.23244	−0.23174
LUMO energy (in H)	−0.11687	−0.11673
HOMO energy (in eV)	−6.325	−6.306
LUMO energy (in eV)	−3.180	−3.176
GAP ΔE (in eV)	3.145	3.130
dipolar moment μ (in Debye)	30.172834	29.529369
average linear polarizability α total (in Bohr^3)	452.941	480.43105
electron affinity A (in a.u.) = $-E_{LUMO}$	0.11687	0.11673
ionization potential I (in a.u.) = $-E_{HOMO}$	0.23244	0.23174
global hardness $\eta = (I - A)/2$	0.057785	0.057505
softness $S = 1/2\eta$	8.652764558	8.694896096
electronegativity $\chi = (I + A)/2$	0.174655	0.174235
electrophilicity index $\omega = \chi^2/2\eta$	0.263947123	0.263958223

[a]Computations have been done at the 6-311G(d,p)/B3LYP level of theory with the IEFPCM water continuum solvent model.

and LUMO is an important stability index and thus an indicator of chemical reactivity. In the hard−soft acid−base principle of Pearson,[38] hardness η is directly related to the gap energy. Electron affinity *A*, ionization potential *I*, global hardness η, and electronegativity χ are unsignificantly higher for idarubicin.
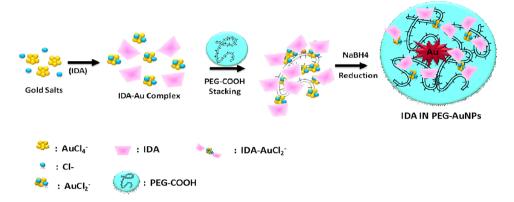
The molecular electrostatic surface potential (MESP) is the plot of electrostatic potential mapped on the total density surface (Figure 3). Different values of the electrostatic potential on the surface are represented by a colored scale: red color represents zero and negative electrostatic potential, whereas the most positive electrostatic potential regions are represented in blue, indicating the major nucleophilic active centers. Mulliken charges for idarubicin and doxorubicin are represented in Figure S2 in the Supporting Information.

Globally, the DFT method predicts that the gap values of approximately 0.116 a.u. are very low, indicating low chemical stability and high polarizability for the two analogs. The low values of ionization energies confirm their high reactivity. Low values of electronegativity χ indicate the low capacity of attracting electrons, whereas the high softness η values indicate a great capacity to receive electrons from the neighboring molecules. HOMO and LUMO are mainly constructed from π orbitals centered on B and C rings (see Scheme S1 in the Supporting Information). Mulliken charges and red-colored electrostatic potential are located around C11 and C12. It confirms the location of interaction and thus complexation with Au (III) ionic species.

In accordance with these interesting results, we designed and conceived an idarubicin hybrid gold nanovector based on Method IN.[7] After full geometry optimizations in gas and water, comparison of the calculated and experimental geometrical parameters reveals only minor differences; thus, the optimized structure is used for further computing analysis.

Formation Mechanism and Physicochemical Characterization of IDA INPEG-AuNPs. Previously, Spadavecchia's group has realized a novel methodology to design new nanotherapeutic agents and hybrid gold nanomaterials based on a gold−biomolecule complex called Method IN.[7] Some authors have conceived the mechanism of hybrid nanoparticles with different capping agents.[39] Actually, no study has been carried out on the formation and synthesis of IDA gold

Scheme 1. Schematic Representation of IDA IN-PEG-AuNPs Synthesis by Complexation of Gold Salt and Drug (Method IN) (All Images Are Not in Scale)

nanoparticles and their chemical and physical characterization starting from the molecular IDA crystallographic structure. Comparison of the experimental and theoretical results based on doxorubicin in our previous study[7] with idarubicin-based results can help us understand their differences in terms of therapeutic activity but also in terms of chemical reactivity. Idarubicin (IDA) is clearly more lipophilic than doxorubicin (DOX). Nevertheless, the presence of the same sugar moiety should yield the electrostatic interactions as those provided for DOX.[40] Previous studies have demonstrated that idarubicin at a concentration fixed to 2×10^{-3} M is present in monomeric species, while doxorubicin exists in dimeric species. The molecular shape of the anthracyclines is determined by (i) the conformation of the sugar ring, (ii) the conformation of the A ring, and (iii) the orientation of the sugar with respect to the aglycone moiety.[41]

Synthesis of IDA INPEG-AuNPs is depicted in Scheme 1. The first step shows the Au (III)−IDA complexation and formation of gold clusters. In the second step, PEG molecules interact electrostatically with Au (III)−IDA complexes. The final reduction with NaBH$_4$ and the growth of AuNPs occur in the third step. All products were evaluated by UV−Vis absorption spectroscopy, TEM, Raman spectroscopy, and ^{1}H NMR.

Physicochemical Evaluation of IDA IN-PEG-AuNPs. Idarubicin (IDA) is a chemical doxorubicin (DOX) analogs except for two groups in the chemical structure (Scheme S1 in the Supporting Information). The differences are highlighted in a table.

In particular, IDA displays a hydroxyl functional group on carbon 10 and a chetone side. In previous studies, IDA was embedded in poly(lactic-co-glycolic-acid) (PLGA) and recently evolved maleate-polyester (MPE) nanoparticles.[42] In the present paper, IDA was chelated to the AuCl$_4^-$ solution to form hybrid gold clusters as described previously.[16] The addition of PEG diacid molecules in the reaction implies the initial reduction process of the nanoparticles.

UV−Vis absorption spectroscopy analysis of the first step (IDA-AuCl$_2^-$ (Figure 4A and Figure 5, black line) showed a characteristic absorption band.[11] We observe a pronounced UV−Vis absorption peak at 302 and 242 nm. The latter one is associated to $\pi-\pi^*$ electronic transitions due to interactions between the IDA ring and gold salt ions[34] and gives clear evidence of the complex formation, in agreement with NMR results (Table 4). This result confirmed that IDA was effectively involved in the nucleation process and creates a
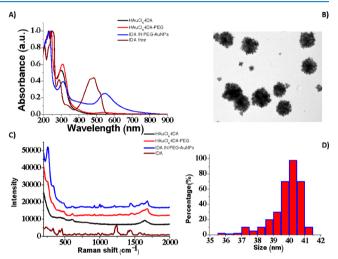

Figure 4. (A) Normalized UV−Vis absorption of IDA IN-PEG-AuNPs (blue line) and their precursor products (HAuCl$_4$-IDA (black line) and HAuCl$_4$-IDA-PEG (red line)) in the range of 200−900 nm. The UV−Vis absorption spectrum of IDA (purple line) is also aincluded for comparison. (B) TEM image of IDA IN-PEG-AuNPs. (C) Raman spectra of the IDA IN-PEG-AuNPs compared to free IDA and their precursor products in the range of 200−2000 cm^{-1}. Experimental conditions: λ_{exc} = 785 nm; laser power, 20 mW; accumulation time, 180 s. (D) Size distribution histogram.

complex with Au. In addition, theoretical results including the computed UV−Visible spectrum (Figure S6 and Table S2 in the Supporting Information) and representation of the molecular orbitals involved in the most intensive transitions (Figures S3−S5 in the Supporting Information) are available in the Supporting Information. In particular, the experimental shifts are in accordance with computations.

In the second step, PEG diacid is added in the IDA-AuCl$_2^-$ solution, leading to the formation of IDA-AuCl$_2$−PEG diacid complexes. A prominent peak at 570 nm in the UV−Vis absorption spectrum of products is visible. This band is largely red-shifted compared to the spectrum corresponding to the first step, which demonstrates the formation of electrostatic interactions between PEG chains and Au (III)−IDA complexes (Figure 4A, red line; Figure 5A, red line; Figure 5A1, red line). In fact, when we focus in the spectral range of 200−400 nm, we observe a red shift to 309 nm, which confirms that the reaction occurs. We believe that, during the second step, Au (III)−IDA complexes migrate through PEG
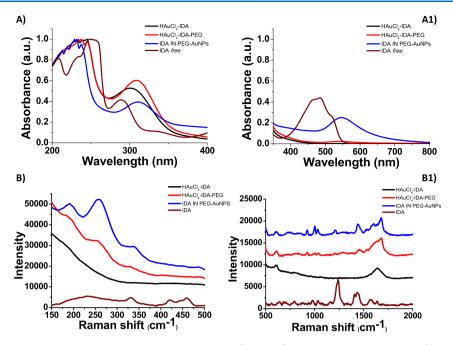
Figure 5. Zoom of normalized UV−Vis absorption of IDA IN PEG-AuNPs (blue line) and their precursor products (HAuCl$_4$-IDA (black line) and HAuCl$_4$-IDA-PEG (red line)) in the ranges of (A) 200−400 nm and (B) 400−800 nm. The UV−Vis absorption spectrum of IDA is also included for comparison. Raman spectra of the IDA IN PEG-AuNPs compared to free IDA in the ranges of (B) 200−500 cm^{-1} and (B1) 500−2000 cm^{-1}. Experimental conditions: λ_{exc} = 785 nm; laser power, 20 mW; accumulation time, 180 s.

Table 4. ^{1}H and ^{13}C Chemical Shifts (in ppm) of Idarubicin in D$_2$O to 300 K

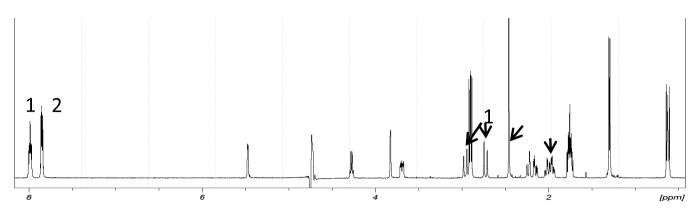| H1/C1	H4/C4	H2/C2	H3/C3	H7/C7	H8′−H8″/C8	H10′−H10″/C10	H14/C14	H1*/C1*	H2*/C2*	H3*/C3*	H4*/C4*	H5*/C5*	H6*/C6*
7.98/126.49	7.98/126.49	7.85/135.22	7.85/135.22	4.79/135.22	4.79/69.1	2.15−2.23/34.8	2.72−2.23/31.36	5.47/99.1	2.00/27.39	3.69/46.64	3.83/66.09	4.27/66.71	1.29/15.52

molecules.[7] Finally, the reduction mixture with NaBH$_4$ was used in the third step to reduce gold species from Au^{III} to Au^0 and form the final product IDA IN-PEG-AuNPs. The reduction of Au proceeds via an electron transfer on the surface of electron-rich, IDA-AuCl$_2$-PEG molecule-capped gold particles with a diameter of 40 nm.[44]
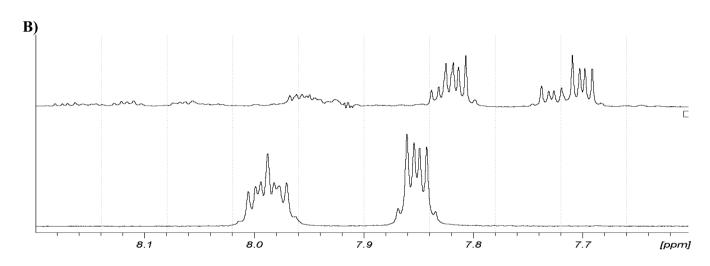
The absorption spectra of IDA IN-PEG-AuNPs were characterized by a small red shift at 312 nm and a blue shift of the surface plasmon band at 546 nm (Figure 4A, blue line; Figure 5A, blue line; Figure 5A1, blue line). TEM images of IDA INPEG-AuNPs display a snow-like shape and good dispersion of the nanoparticles with an average size of 40 ± 1 nm (Figure 4B,D).The characteristic flower shape obtained is very different from doxorubicin gold nanoparticles (DOX IN-PEG-AuNPs) previously described,[7] which confirms a different steric orientation of IDA onto the crystallographic gold facet. Other authors have realized that the synthesis of similar nanostructures added macromolecules and biopolymer molecules in the growth solution of AuNPs.[43] Based on previous reported findings,[44,45] we suppose that, when IDA and dicarboxylic PEG were added to the AuCl$_4^-$ solution, the PEG was bound initially to Au (III) in a mushroom conformation.[10]

In addition, the bright pink-violet color of both nanoparticles and the UV−Vis spectra remain unaltered after storage for more than 3 months at room temperature, suggesting the formation of a stable particle suspension. The NP sizes were confirmed by DLS measurements. Zeta potential measurements show that IDA IN was colloidally stable at physiological pH (z-potential = −25 ± 1 MV with a PdI equal to 0.241). In monomeric anthracycline derivatives, in aqueous solution, the mean plane of the sugar is perpendicular to the dihydroxy anthraquinone plane. This property influence the steric conformation of idarubicin, which is more deeply embedded within a bilayer of polymer than DOX, forming a rather complex entity involving two to three molecules of idarubicin associated in the right-handed conformation.[40] The steric arrangement of IDA during the synthetic process of PEGylated gold nanoparticles was confirmed by Raman spectroscopic analysis (Figure 4C).

In detail, the Raman spectra of free IDA (Figure 4C, purple line) and IDA IN-PEG-AuNPs (Figure 4C, blue line) in water exhibit many bands in the region 500−2000 cm.$^{-1}$The wide band observed around 1600 cm^{-1} on the Raman spectra is assigned to water. Previous studies have demonstrated remarkable differences between the Raman spectra of doxorubicin before and after complexation with biomolecules or metal.[7] Considering the spectra of IDA IN-PEG-AuNPs, the resonance bands at 1205, 1445, and 1595 cm^{-1}, corresponding to the ν_{C-O} and $\nu_{C=C}$) vibration of ring A, are responsible for the variation in the steric conformation of IDA. The bands at 1445 and 430 cm^{-1} become more prominent upon complexation. The resonance bands at 1275, 1420, and 1516 cm^{-1}, corresponding to the ν_{C-O} and $\nu_{C=C}$ vibration of ring A, are responsible for the variation in the steric conformation of DOX. Indeed, when C=O and hydroxyl groups of IDA interact with a metal, the conformation of the drug becomes
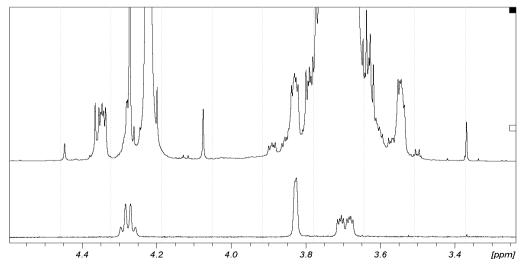
A)

B)

Figure 6. (A) ^{1}H NMR spectra of idarubicin at 300 K and (B) extended area of ^{1}H NMR spectra of idarubicin (1) and IDA IN-PEG-AuNPs (2) at 300 K.

more inclined to a perpendicular orientation rather than to a flat one.[7]

The Raman fingerprint of the first step (IDA-AuCl$_2$$^-$) product was the presence of a peak around 350 and 460 cm^{-1} due to complexation. Indeed, this band can be assigned to the

gold chloride stretches and δ(O−Au−O) in ring F. The Raman spectrum of IDA IN-PEG-AuNPs (Figure 1C, blue line) was comparable to that of the intermediate product (IDA-AuCl$_2$$^-$-PEG; Figure 1C, red line), with the exception of new bands between 700 and 900 cm^{-1} and around 1580 cm^{-1}.

Table 5. ^{1}H and ^{13}C Chemical Shifts (in ppm) of IDA IN-PEG-AuNPs in D$_2$O to 300 K^a

H1(m)/C1	H4(m)/C4	H2(q)/C2	H3(q)/C3	H7(s)/C7	H8′(s)−H8″(s)/C8	H10′(s)−H10″(s)/C10	H14(s)/C14	H1*(d)/C1*	H2*(d)/C2*	H3*(m)/C3*	H4*(s)/C4*	H5*(q)/C5*	H6*(d)/C6*
7.95/135.66	7.81/128.93	7.69/131.88	7.72/132.12	#/#	2.10−2.20/34.82	2.80/31.36	2.35/24.23	5.80/90	2.00/27.5	#/#	#/#	4.33/64.17	1.22/15.78

^{a}#, masked by PEG.

Such bands were attributed to IDA aromatic ring vibrations and to those of C=O and hydroxyl groups in the IDA molecule. It has already been described that most of the Raman bands of molecules can be significantly enhanced by their proximity to the surface AuNPs. Moreover, we also assume that the IDA−Au interaction is still the same after the NP formation and that IDA is grafted on the NP surface through the complex formation with Au. The steric orientation of IDA on the AuNP surface will be influenced by electrostatic interactions between the amino group and phenol in the presence of diacidic PEG molecules under a specific condition of pH and ionic strength. Focusing our attention on the zoom spectral ranges of 200−500 cm^{-1} (Figure 2A) and 5000−2000 cm^{-1} (Figure 2B), one can detect several spectral changes, which confirms a chemical and steric modification of the drug (IDA) after complexation with gold ions and PEG diacid molecules. One of the Raman fingerprints of the IDA IN-PEG-AuNPs is the presence of a double peak at 189−257 cm^{-1} (Figure 4C). These bands can be assigned to the gold chloride stretches, ν(Au−Cl), and δ(O−Au−O) and are clear evidence of the formation of a complex between AuCl$_2^-$ and IDA in solution. The common peak at 342 cm^{-1} is due to the vibrations δ(OH···O) and ν(OH···O) of the PEG. Therefore, we suggest that, during the reduction process, NaBH$_4$ reduced Au^{3+} to Au^0 to form dispersed AuNPs of relatively uniform size in which IDA was entrapped between PEG chains and AuNPs. We assume that this behavior is due to steric arrangement of the IDA−Au complex into PEG molecules. This phenomena influence the drug-surface orientation with change in electronic distribution within the IDA, Au^{3+}, and PEG chains during the synthetic process with formation of a new drug−gold nanoparticle system.

Otherwise, the ^{1}H NMR spectrum of IDA IN-PEG-AuNPs (Figure 6)A showed important signals of PEG versus the IDA signals (3.64 (s, 14H) and 3.66 to 3.70 ppm (m, 4H)), which mask some chemical shifts of proton of IDA. This prevents us from confirming the Raman data.

^{1}H NMR Characterization. Figure 6A shows the ^{1}H NMR spectra of IDA and the complex IDA INPEG-AuNPs. The ^{1}H and ^{13}C assignments are presented in Tables 4 and 5, respectively.

Unfortunately, the other intermediates of each synthetic step were not concentrated enough on the NMR scale to be detected. As shown in Figure 6, the major change between the IDA spectrum and IDA IN-PEG-AuNPs spectrum is located in the aromatic area peaks (7.2 to 7.8 ppm), suggesting that IDA was complexed by forming bonds between aromatic protons of the ring and AuCl$_2$. The rest of the chemical shifts are similar from one spectrum to another, but the ^{1}H NMR spectrum of IDA IN-PEG-AuNPs showed intense signals of PEG. The ^{1}H NMR spectrum of IDA IN-PEG-AuNPs showed important signals of PEG versus the IDA signals (3.64 (s, 14H) and 3.66 to 3.70 ppm (m, 4H)), which mask some chemical shifts of proton of IDA. This prevents us from confirming the Raman data.

Loading, Release, and Stability of IDA INPEG-AuNPs. The successful loading ratio of IDA into PEG-AuNPs was evidenced by the characteristic absorption peaks at 485 nm (Figure S1A). The standard absorption of IDA was plotted in the inset of the figure (Figure S1B) according to the UV−Vis absorbance spectra of IDA at various concentrations and perfectly identical to DOX loaded in the previous work.[7] The loading efficiency was estimated to be 83% with 8.0 μg of IDA present in 2.4 × 10^{-7} mol of NPs (data not shown). The stability of IDA IN-PEG-AuNPs in solution was monitored by the localized surface plasmon (LSP) band of the AuNPs (Figure S8 in the Supporting Information). Analysis was performed in DMEM and under ionic strength conditions over a period of time (3 months). A red shift of the LSP band confirms an increase in the size of the particle or an aggregation of nanoparticles.

The synthesized IDA IN-PEG-AuNPs did show an almost negligible change in the LSP band position over a period of 3 months (Figure S8 in the Supporting Information).

Although the LPS band intensity slightly decreased over time, we could conclude that no major agglomeration occurred over 2 months, implying that IDA IN-PEG-AuNPs might find application as clinical drug-delivery systems.

CONCLUSIONS

The achievement of this study was to provide design, synthesis, and characterization of new nanotherapeutics based on a stable Au (III)−idarubicin complex. The crystal structure of IDA by X-ray diffraction measurements on single crystals was obtained for the first time in the literature and the theoretical study was proved. In our paper, Raman spectroscopy and ^{1}H NMR analysis of IDA molecules were realized during chelation reaction to understand the drug orientation during the formation of hybrid nanoparticles. All experimental results were simulated by density functional theory (DFT) and time-dependent density functional theory (TD-DFT) method to support the spectral shifts observed experimentally. The "nanodrug complex" exhibits many advantages as nanotherapeutic for cancer therapy, including (i) solubility and high drug loading, (ii) specific release under pH conditions, and (iii) stability in DMEM solution. These findings highlight the potential of the SERS approach to study IDA−gold interactions in relation to drug delivery and drug biological activity.

EXPERIMENTAL SECTION

Materials. All chemical materials were acquired from Sigma-Aldrich (Saint-Quentin Fallavier, France) as described in a previous article[11] and Eurisotop for D$_2$O.

Synthesis of IDA IN-PEG-AuNPs. Synthesis of IDA IN-PEG-AuNPs colloids included three main steps, as depicted in Scheme 1. Twenty milliliters of HAuCl$_4$ solution (2.5 × 10^{-4}

M) was mixed to IDA (5 mL, 1.54×10^{-4} M in water) and stirred for 20 min. After this time, 250 μL of dicarboxylic PEG was added.[10] Finally, 600 μL of aqueous 0.02 M NaBH$_4$ was added at once. The formation of the IDA IN-PEG-AuNPs was observed as an instantaneous color change of the solution from pale yellow to pink-purple after addition of the reducing agent. All chemical intermediates of each synthetic step were characterized by UV−Vis spectroscopy, transmission electron microscopy (TEM), ^{1}H NMR, and Raman spectroscopy. The "as-prepared" IDA IN-PEG-AuNPs solution was purified as described previously.[10]

Physicochemical Characterization. All characterizations were carried out in triplicate to corroborate the reproducibility of the synthetic and analytical procedures as previously described.[10]

X-ray Diffraction Measurements. Single crystals suitable for X-ray structure analysis were obtained after 1 week by slow evaporation at 278 K from a concentrated IDA ethanolic solution (5 mg/mL). Suitable crystals were mounted for measurements. A complete data collection was performed at room temperature on a Rigaku microsource MM-003 diffractometer using Mo Kα ($\lambda = 0.71073$ Å) radiation and processed with the CrysAlis PRO package of programs.[11] The crystal structure was solved with direct methods using SIR-92 and final refinement based on F^2 and was carried out by full-matrix least squares with SHELXL-2018 software[11] and WINGX gui.[12] Refinement was performed anisotropically for all nonhydrogen atoms. In the final stages of least-squares refinement, hydrogen atoms were assigned to idealized positions and allowed to ride with thermal parameters fixed at 1.2 Ueq of the parent atom.

The CCDC 2027730 record contains the supplementary crystallographic data for this paper. These data can be obtained free of charge from The Cambridge Crystallographic Data Centre via https://www.ccdc.cam.ac.uk/structures/.

^{1}**H NMR.** Experiments were conducted on an AVANCE III spectrometer (Bruker Biospin, Wissembourg, France) operating at 500 MHz with a 5 mm gradient indirect detection probe at a probe temperature of 300 K. Thirty-two scans were acquired to generate the spectra of IDA (5 mM) and IDA IN-PEG-AuNPs (2 mM). The data acquisition size was 32k and the spectral width was 5000 Hz. A typical 8.7 μs pulse length and relaxation delay of 2 s were used. The water signal was suppressed by applying a secondary irradiation field at the water resonance frequency (presaturation sequence). The dried idarubicin and the complex were resuspended in 600 μL of deuterium oxide (D$_2$O) (99.96%, Eurisotop) containing 5 mM 2-dimethyl-2-silapentane-5-sulfonic acid (DSS) as an internal reference. Samples were placed in 5 mm diameter tubes for ^{1}H NMR analysis. For ^{1}H resonance assignment, the COSY spectra were acquired for IDA with 4k data points and 32 transients for each of the 128 increments and 64 transients/ 256 increments for IDA IN-PEG-AuNPs. Moreover, 2D NMR HSQC experiments were performed for ^{13}C bound to the proton resonance assignment. Chemical shifts (δ, in ppm) were compared to the NMR solvent signal DSS (0 ppm at 300 K).

Dynamic Light Scattering (DLS). All measurements were carried out as previously described.[10]

Zeta Potential Measurements. All measurements were carried out as previously described.[10]

IDA Loading Efficiency. The amount of the drug incorporated into IDA IN-PEG-AuNPs was measured by UV−Vis absorption spectroscopy. Absorption at 485 nm was used to extrapolate IDA concentrations based on a calibration curve (Figure S1 in the Supporting Information).

Stability of IDA IN-PEG-AuNPs. The stability of nanoparticles was monitored by UV−Vis. IDA IN-PEG-AuNPs were dissolved in DMEM for 48 h (Figure S8 in Supporting Information).

Density Functional Theory Calculations (DFT). DFT calculations based on initial molecular files of molecular IDA and IDA complexed in the presence of Au (III) were done as described before with doxorubicin.[7] In addition, a system associating a small Au$_6$ cluster and an idarubicin molecule representing the first step of nanoparticle growth was considered. Presently, the PEG molecular effect was not taken in account. All molecular calculations were performed in the gas phase and in water as previously described. The solvent effect on energies was included using the IEFPCM continuum model[13] as implemented in the Gaussian 16 suite of program.[14] All geometries were fully optimized without any symmetry constraints using the density functional theory at the hybrid functional B3LYP level.[15−17] The B3LYP method with the 6-311G(d,p) basis set is commonly used in predicting the vibrational spectra of polyaromatic molecules.[18]

The standard split valence basis set 6-311G(d,p) was used for all atoms, except for Au and Cl, which were treated by the relativistic effective core potential (ECP) and associated valence double-ξ basis set of Hay and Wadt (abbreviated as LANL2DZ).[19] After structural optimizations, vibrational frequencies and Raman scattering were computed at the same level of density functional theory GaussSum 3.0.[20]

DFT calculations were used to generate Raman intensities with a 785 nm excitation wavelength and full width at half-maximum parameter of 20 cm^{-1}. The calculated harmonic Raman vibrational wavenumbers were scaled down uniformly.[21] UV−Vis transition was finally evaluated in the gas phase and in water with a PCM model using the time-dependent (TD) approach[22] at the same level of DFT. Three structures were considered (Figure 3): idarubicin sI (named IDA), a square-planar Au (III) dichloro-idarubicin complex sII (named IDAAuCl$_2$), and a system associating a small Au$_6$ cluster and an idarubicin molecule sIII (named IDA-Au$_6$). The trigonal plane Au$_6$-clustered structure is directly inspired from previous publications.[23−25] Please note that only relevant results are mentioned in the main text, whereas most of the computed data are reported in the Supporting Information. In addition, the electrostatic potential (ESP) and corresponding contour maps (MESP) have been considered for structures sI to sIII. To emphasize the differences between the atomic sites, the blue areas have been constructed from negative to positive electrostatic potential values.

In the following part of the text, DFT computations will help the Raman band understandings, while TD-DFT (time-dependent density functional theory) computations will guide the UV−Visible band assignments for the three steps of synthesis from the molecular state in solution to the gold nanoparticle formation.

■ ASSOCIATED CONTENT

ⓢ Supporting Information

The Supporting Information is available free of charge at https://pubs.acs.org/doi/10.1021/acsomega.0c04501.

Chemical difference in structures between IDA and doxorubicin rings; UV−Vis absorption spectra of IDA at increasing known concentrations and the amount of IDA molecules contained in IDA IN-PEG-AuNPs; computed Mulliken charge model distribution for sI (IDA) and doxorubicin; graphical representations of molecular orbitals involved in the more intensive UV−Vis electronic transition for sI (IDA), sII (IDA-AuCl$_2$), and sIII (IDA-Au$_6$); comparison of scaled computed and experimental UV−Visible spectra for sI to sIII and different experimental steps; graphical superimposition of experimental and calculated Raman spectra for sI to sIII and different experimental steps; stability of IDA IN-PEG-AuNPs in DMEM as a function of time; principal chemical descriptors for sI and sII structures optimized by DFT/B3LYP/IEFPCM in water and for DOX and DOXAuCl$_2$ for comparison; calculated UV−Visible electronic transitions and assignments for sI and sIII structures at the B3LYP/6-311G(d,p)/LANL2DZ TD-DFT level of theory (PDF)

AUTHOR INFORMATION

Corresponding Author

Jolanda Spadavecchia − *CNRS, UMR 7244, NBD-CSPBAT, Laboratoire de Chimie, Structures et Propriétés de Biomatériaux et d'Agents Thérapeutiques Université Sorbonne Paris Nord, Bobigny 93000, France;* ⊙ orcid.org/ 0000-0001-6697-1174; Email: jolanda.spadavecchia@ univ-paris13.fr, jolanda.spadavecchia@gmail.com

Authors

Carole Barbey − *CNRS, UMR 7244, NBD-CSPBAT, Laboratoire de Chimie, Structures et Propriétés de Biomatériaux et d'Agents Thérapeutiques Université Sorbonne Paris Nord, Bobigny 93000, France*

Nadia Bouchemal − *CNRS, UMR 7244, NBD-CSPBAT, Laboratoire de Chimie, Structures et Propriétés de Biomatériaux et d'Agents Thérapeutiques Université Sorbonne Paris Nord, Bobigny 93000, France*

Pascal Retailleau − *CNRS, UPR 2301, Service de Cristallochimie, Institut des Substances Naturelles, Gif sur Yvette 91190, France*

Nathalie Dupont − *CNRS, UMR 7244, NBD-CSPBAT, Laboratoire de Chimie, Structures et Propriétés de Biomatériaux et d'Agents Thérapeutiques Université Sorbonne Paris Nord, Bobigny 93000, France*

Complete contact information is available at:
https://pubs.acs.org/10.1021/acsomega.0c04501

Author Contributions

The manuscript was written through contributions of all authors. All authors have given approval to the final version of the manuscript.

Notes

The authors declare no competing financial interest.

ACKNOWLEDGMENTS

REFERENCES

(1) Shaul, P.; Frenkel, M.; Goldstein, E. B.; Mittelman, L.; Grunwald, A.; Ebenstein, Y.; Tsarfaty, I.; Fridman, M. The structure of anthracycline derivatives determines their subcellular localization and cytotoxic activity. *ACS Med. Chem. Lett.* **2013**, *4*, 323−328.

(2) Alvarez-Cardona, J.; Lenihan, D. J. Anthracycline Cardiotoxicity: It Is Possible to Teach an Old Dog Some New Tricks. *Cardiol. Clin.* **2019**, *37*, 355−363.

(3) Salvatorelli, E.; Guarnieri, S.; Menna, P.; Liberi, G.; Calafiore, A. M.; Mariggiò, M. A.; Mordente, A.; Gianni, L.; Minotti, G. Defective one- or two-electron reduction of the anticancer anthracycline epirubicin in human heart. Relative importance of vesicular sequestration and impaired efficiency of electron addition. *J. Biol. Chem.* **2006**, *281*, 10990−11001.

(4) Weiss, R. B.; Sarosy, G.; Clagett-Carr, K.; Russo, M.; Leyland-Jones, B. Anthracycline analogs The past, present, and future. *Cancer Chemother. Pharmacol.* **1986**, *18*, 185−197.

(5) Groom, C. R.; Bruno, I. J.; Lightfoot, M. P.; Ward, S. C. The Cambridge Structural Database. *Acta Crystallogr., Sect. B: Struct. Sci., Cryst. Eng. Mater.* **2016**, *72*, 171−179.

(6) Berman, H. M.; Westbrook, J.; Feng, Z.; Gilliland, G.; Bhat, T. N.; Weissig, H.; Shindyalov, I. N.; Bourne, P. E. The Protein Data Bank. *Nucleic Acids Res.* **2000**, *28*, 235−242.

(7) Moustaoui, H.; Movia, D.; Dupont, N.; Bouchemal, N.; Casale, S.; Djaker, N.; Savarin, P.; Prina-Mello, A.; de la Chapelle, M. L.; Spadavecchia, J. Tunable Design of Gold(III)−Doxorubicin Complex−PEGylated Nanocarrier. The Golden Doxorubicin for Oncological Applications. *ACS Appl. Mater. Interfaces* **2016**, *8*, 19946−19957.

(8) Marguerit, G.; Moustaoui, H.; Haddada, M. B.; Djaker, N.; de la Chapelle, M. L.; Spadavecchia, J. Taxanes Hybrid Nanovectors: From Design to Physico-Chemical Evaluation of Docetaxel and Paclitaxel Gold (III)-PEGylated Complex Nanocarriers. *Part. Part. Syst. Charact.* **2018**, *35*, 1700299.

(9) Sahli, F.; Courcelle, M.; Palama, T.; Djaker, N.; Savarin, P.; Spadavecchia, J. Temozolomide, Gemcitabine, and Decitabine Hybrid Nanoconjugates: From Design to Proof-of-Concept (PoC) of Synergies toward the Understanding of Drug Impact on Human Glioblastoma Cells. *J. Med. Chem.* **2020**, *63*, 7410−7421.

(10) Spadavecchia, J.; Movia, D.; Moore, C.; Maguire, C. M.; Moustaoui, H.; Casale, S.; Volkov, Y.; Prina-Mello, A. Targeted polyethylene glycol gold nanoparticles for the treatment of pancreatic cancer: from synthesis to proof-of-concept in vitro studies. *Int. J. Nanomed.* **2016**, *11*, 791−822.

(11) Nicholls, D.; Elleman, C.; Shankland, N.; Shankland, K. A new crystalline form of αβ-d-lactose prepared by oven drying a concentrated aqueous solution of d-lactose. *Acta Crystallogr., Sect. C: Struct. Chem.* **2019**, *75*, 904−909.

(12) Farrugia, L. J. WinGX and ORTEP for Windows: an update. *J. Appl. Crystallogr.* **2012**, *45*, 849−854.

(13) Tomasi, J.; Mennucci, B.; Cammi, R. Quantum Mechanical Continuum Solvation Models. *Chem. Rev.* **2005**, *105*, 2999−3094.

(14) Frisch, M. J.; Trucks, G. W.; Schlegel, H. B.; Scuseria, G. E.; Robb, M. A.; Cheeseman, J. R.; Scalmani, G.; Barone, V.; Petersson, G. A.; Nakatsuji, H.; Li, X.; Caricato, M.; Marenich, A. V.; Bloino, J.; Janesko, B. G.; Gomperts, R.; Mennucci, B.; Hratchian, H. P.; Ortiz, J. V.; Izmaylov, A. F.; Sonnenberg, J. L.; Williams; Ding, F.; Lipparini, F.; Egidi, F.; Goings, J.; Peng, B.; Petrone, A.; Henderson, T.; Ranasinghe, D.; Zakrzewski, V. G.; Gao, J.; Rega, N.; Zheng, G.; Liang, W.; Hada, M.; Ehara, M.; Toyota, K.; Fukuda, R.; Hasegawa, J.; Ishida, M.; Nakajima, T.; Honda, Y.; Kitao, O.; Nakai, H.; Vreven, T.; Throssell, K.; Montgomery, J. A., Jr.; Peralta, J. E.; Ogliaro, F.; Bearpark, M. J.; Heyd, J. J.; Brothers, E. N.; Kudin, K. N.; Staroverov, V. N.; Keith, T. A.; Kobayashi, R.; Normand, J.; Raghavachari, K.; Rendell, A. P.; Burant, J. C.; Iyengar, S. S.; Tomasi, J.; Cossi, M.; Millam, J. M.; Klene, M.; Adamo, C.; Cammi, R.; Ochterski, J. W.; Martin, R. L.; Morokuma, K.; Farkas, O.; Foresman, J. B.; Fox, D. J. *Gaussian 16 Rev. C.01*, Wallingford, CT, 2016.

(15) Becke, A. D. Density-functional exchange-energy approximation with correct asymptotic behavior. *Phys. Rev. A* **1988**, *38*, 3098−3100.

(16) Lee, C.; Yang, W.; Parr, R. G. Development of the Colle-Salvetti correlation-energy formula into a functional of the electron density. *Phys. Rev. B: Condens. Matter* **1988**, *37*, 785−789.

(17) Becke, A. D. Density-functional thermochemistry. IV. A new dynamical correlation functional and implications for exact-exchange mixing. *J. Chem. Phys.* **1996**, *104*, 1040.

(18) Shakila, G.; Periandy, S.; Ramalingam, S. Molecular Structure and Vibrational Analysis of 1-Bromo-2-Chlorobenzene Using ab initio HF and Density Functional Theory (B3LYP) Calculations. *J. At. Mol. Phys.* **2011**, *2011*, 512841.

(19) Hay, P. J.; Wadt, W. R. *Ab initio* effective core potentials for molecular calculations. Potentials for the transition metal atoms Sc to Hg. *J. Chem. Phys.* **1985**, *82*, 270−283.

(20) O'Boyle, N. M.; Tenderholt, A. L.; Langner, K. M. cclib: a library for package-independent computational chemistry algorithms. *J. Comput. Chem.* **2008**, *29*, 839−845.

(21) Scott, A. P.; Radom, L. Harmonic Vibrational Frequencies: An Evaluation of Hartree−Fock, Møller−Plesset, Quadratic Configuration Interaction, Density Functional Theory, and Semiempirical Scale Factors. *J. Phys. Chem.* **1996**, *100*, 16502−16513.

(22) Stratmann, R. E.; Scuseria, G. E.; Frisch, M. J. An efficient implementation of time-dependent density-functional theory for the calculation of excitation energies of large molecules. *J. Chem. Phys.* **1998**, *109*, 8218−8224.

(23) Khatun, M.; Majumdar, R. S.; Anoop, A. A Global Optimizer for Nanoclusters. *Front. Chem.* **2019**, *7*, 644−644.

(24) Cheng, L.; Xiao-Yu, K.; Zhi-Wen, L.; Ai-Jie, M.; Yan-Ming, M. Determination of Structures, Stabilities, and Electronic Properties for Bimetallic Cesium-Doped Gold Clusters: A Density Functional Theory Study. *J. Chem. Phys. A* **2011**, *115*, 9273−9281.

(25) Goel, S.; Velizhanin, K. A.; Piryatinski, A.; Tretiak, S.; Ivanov, S. A. DFT Study of Ligand Binding to Small Gold Clusters. *J. Chem. Phys. Lett.* **2010**, *1*, 927−931.

(26) Mathivathanan, L.; Yang, G.; Leng, F.; Raptis, R. G. Crystal structure and conformational analysis of doxorubicin nitrate. *Acta Crystallogr., Sect. E: Crystallogr. Commun.* **2018**, *74*, 400−405.

(27) Tsoneva, Y.; Jonker, H. R. A.; Wagner, M.; Tadjer, A.; Lelle, M.; Peneva, K.; Ivanova, A. Molecular Structure and Pronounced Conformational Flexibility of Doxorubicin in Free and Conjugated State within a Drug−Peptide Compound. *J. Chem. Phys. Chem. B* **2015**, *119*, 3001−3013.

(28) Zhu, S.; Yan, L.; Ji, X.; Lu, W. Conformational diversity of anthracycline anticancer antibiotics: A density functional theory calculation. *J. Mol. Struct.: THEOCHEM* **2010**, *951*, 60−68.

(29) Cozzi, F.; Ponzini, F.; Annunziata, R.; Cinquini, M.; Siegel, J. S. Polar Interactions between Stacked π Systems in Fluorinated 1,8-Diarylnaphthalenes: Importance of Quadrupole Moments in Molecular Recognition. *Angew. Chem. Int. Ed. Engl.* **1995**, *34*, 1019−1020.

(30) Meyer, E. A.; Castellano, R. K.; Diederich, F. Interactions with aromatic rings in chemical and biological recognition. *Angew. Chem. Int. Ed.* **2003**, *42*, 1210−1250.

(31) Macrae, C. F.; Bruno, I. J.; Chisholm, J. A.; Edgington, P. R.; McCabe, P.; Pidcock, E.; Rodriguez-Monge, L.; Taylor, R.; Van De Streek, J.; Wood, P. A. *Mercury CSD 2.0*− new features for the visualization and investigation of crystal structures. *J. Appl. Crystallogr.* **2008**, *41*, 466−470.

(32) DeVita, V. T.; Steven, A.; Rosenberg, S. A. *DeVita, Hellman, and Rosenberg's cancer: Principles & practice of oncology*; Tenth edition.; Wolters Kluwer Health Adis (ESP): 2015; 1−2280.

(33) Ng, R.; Better, N.; Green, M. D. Anticancer Agents and Cardiotoxicity. *Semin. Oncol.* **2006**, *33*, 2−14.

(34) Sarmah, P.; Deka, R. C. Anticancer activity of nucleoside analogues: a density functional theory based QSAR study. *J. Mol. Model.* **2010**, *16*, 411−418.

(35) Sarmah, P.; Deka, R. C. DFT-based QSAR and QSPR models of several cis-platinum complexes: solvent effect. *J. Comput.-Aided Mol. Des.* **2009**, *23*, 343−354.

(36) Boufas, W.; Dupont, N.; Berredjem, M.; Berrezag, K.; Becheker, I.; Berredjem, H.; Aouf, N.-E. Synthesis and antibacterial activity of sulfonamides. SAR and DFT studies. *J. Mol. Struct.* **2014**, *1074*, 180−185.

(37) Koopmans, T. Über die Zuordnung von Wellenfunktionen und Eigenwerten zu den Einzelnen Elektronen Eines Atoms. *Physica* **1934**, *1*, 104−113.

(38) Pearson, R. G. Hard and Soft Acids and Bases. *J. Am. Chem. Soc.* **1963**, *85*, 3533−3539.

(39) Spadavecchia, J.; Apchain, E.; Albéric, M.; Fontan, E.; Reiche, I. One-step synthesis of collagen hybrid gold nanoparticles and formation on Egyptian-like gold-plated archaeological ivory. *Angew. Chem. Int. Ed.* **2014**, *53*, 8363−8366.

(40) Gallois, L.; Fiallo, M.; Garnier-Suillerot, A. Comparison of the interaction of doxorubicin, daunorubicin, idarubicin and idarubicinol with large unilamellar vesicles: Circular dichroism study. *Biochim. Biophys. Acta, Biomembr.* **1998**, *1370*, 31−40.

(41) Temperini, C.; Messori, L.; Orioli, P.; Di Bugno, C.; Animati, F.; Ughetto, G. The crystal structure of the complex between a disaccharide anthracycline and the DNA hexamer d(CGATCG) reveals two different binding sites involving two DNA duplexes. *Nucleic Acids Res.* **2003**, *31*, 1464−1469.

(42) Blaudszun, A.-R.; Lian, Q.; Schnabel, M.; Loretz, B.; Steinfeld, U.; Lee, H.-H.; Wenz, G.; Lehr, C.-M.; Schneider, M.; Philippi, A. Polyester-idarubicin nanoparticles and a polymer-photosensitizer complex as potential drug formulations for cell-mediated drug delivery. *Int. J. Pharm.* **2014**, *474*, 70−79.

(43) Aouidat, F.; Boumati, S.; Khan, M.; Tielens, F.; Doan, B.-T.; Spadavecchia, J. Design and Synthesis of Gold-Gadolinium-Core-Shell Nanoparticles as Contrast Agent: a Smart Way to Future Nanomaterials for Nanomedicine Applications. *Int. J. Nanomed.* **2019**, *Volume 14*, 9309−9324.

(44) Liu, H.; Jiang, P.; Li, Z.; Li, X.; Djaker, N.; Spadavecchia, J. HIV-1 Tat Peptide-Gemcitabine Gold (III)-PEGylated Complex—Nanoflowers: A Sleek Thermosensitive Hybrid Nanocarrier as Prospective Anticancer. *Part. Part. Syst. Charact.* **2018**, *35*, 1800082.

(45) Liu, Q.; Aouidat, F.; Sacco, P.; Marsich, E.; Djaker, N.; Spadavecchia, J. Galectin-1 protein modified gold (III)-PEGylated complex-nanoparticles: Proof of concept of alternative probe in colorimetric glucose detection. *Colloids Surf., B* **2020**, *185*, 15.